ACS APPLIED MATERIALS & INTERFACES

Research Article

www.acsami.org

Enhanced Power-Conversion Efficiency in Inverted Bulk Heterojunction Solar Cells using Liquid-Crystal-Conjugated Polyelectrolyte Interlayer

Chao Liu,[†] Yun Tan,[†] Chunquan Li,[§] Feiyan Wu,[†] Lie Chen,[*,†,‡] and Yiwang Chen[†,‡]

[†]College of Chemistry/Institute of Polymers, Nanchang University, 999 Xuefu Avenue, Nanchang 330031, China

[‡]Jiangxi Provincial Key Laboratory of New Energy Chemistry, Nanchang University, 999 Xuefu Avenue, Nanchang 330031, China

[§]Department of Electronic Information Engineering, Nanchang University, Nanchang University, 999 Xuefu Avenue, Nanchang 330031, China

Supporting Information

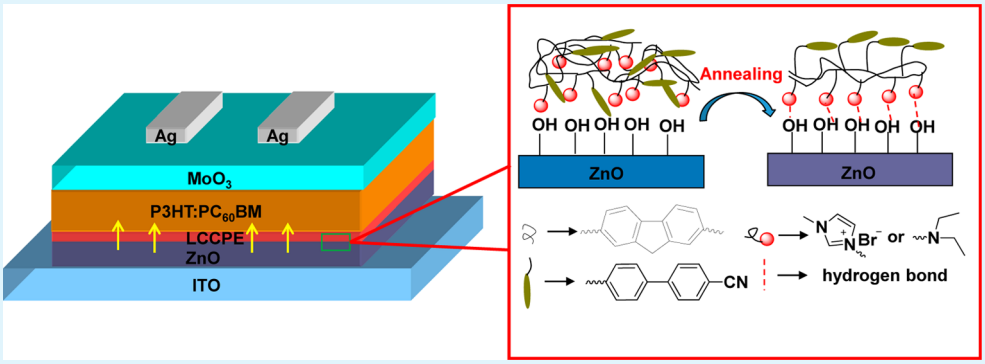

ABSTRACT: Two novel liquid-crystal-conjugated polyelectrolytes (LCCPEs) poly[9,9-bis[6-(4-cyanobiphenyloxy)-hexyl]−fluorene−*alt*-9,9-bis(6-(*N*,*N*-diethylamino)-hexyl)-fluorene] (PF6Ncbp) and poly[9,9-bis[6-(4-cyanobiphenyloxy)-hexyl]−fluorene−*alt*-9,9-bis(6-(*N*-methylimidazole)-hexyl]-fluorene] (PF6lmicbp) are obtained by covalent linkage of the cyanobiphenyl mesogen polar groups onto conjugated polyelectrolytes. After deposition a layer of LCCPEs on ZnO interlayer, the spontaneous orientation of liquid-crystal groups can induce a rearrangement of dipole moments at the interface, subsequently leading to the better energy-level alignment. Moreover, LCCPEs favors intimate interfacial contact between ZnO and the photon harvesting layer and induce active layer to form the nanofibers morphology for the enhancement of charge extraction, transportation and collection. The water/alcohol solubility of the LCCPEs also enables them to be environment-accepted solvent processability. On the basis of these advantages, the poly(3-hexylthiophene) (P3HT):[6,6]-phenyl-C_{60}-butyric acid methyl ester ($PC_{60}BM$)-based inverted polymer solar cells (PSCs) combined with ZnO/PF6Ncbp and ZnO/PF6lmicbp bilayers boost the power conversion efficiency (PCE) to 3.9% and 4.2%, respectively. Incorporation of the ZnO/PF6lmicbp into the devices based on a blend of a narrow band gap polymer thieno[3,4-*b*]thiophene/benzodithiophene (PTB7) with [6,6]-phenyl C_{70}-butyric acid methyl ester (PC71BM) affords a notable efficiency of 7.6%.

KEYWORDS: *liquid crystal, conjugated polyelectrolytes, interfacial modification, polymer solar cells, inverted devices*

1. INTRODUCTION

Bulk-heterojunction (BHJ) polymer solar cells (PSCs) are promising devices for their potential to obtain inexhaustible energy source. Researches on them have received great attention because of their capability for large-scales, low cost, and mechanical flexibility.[1−3] Recently, highly effective polymer solar cells have been obtained with an inverted device configuration using high work-function anode (e.g., Au, Ag) to collect holes and modified indium tin oxide (ITO) as the cathode to collect electrons.[4] Compared to the traditional PSCs, inverted devices present superior long-term humid stability by averting the usage for the hygroscopic and corrosive hole-transmission layer material poly(3,4-ethylenedioxylenethiophene):poly(styrenesulfonic acid) (PEDOT:PSS) and low work-function metal cathode, both of which are prejudicious to device longevity.[5−8]

In the inverted configuration with bare ITO cathode, the polymer−fullerene solar cells demonstrate inferior performance because of the mismatch between the high work function of the ITO (~4.8 eV) and the lowest unoccupied molecular orbital (LUMO ≈ 4.0 eV) of the fullerene acceptor in active layer.[9] The zinc oxide (ZnO),[10] titanium oxide (TiOx),[4,11] and cesium

Received: April 17, 2015
Accepted: August 17, 2015
Published: August 17, 2015

DOI: 10.1021/acsami.5b03340
ACS Appl. Mater. Interfaces 2015, 7, 19024−19033

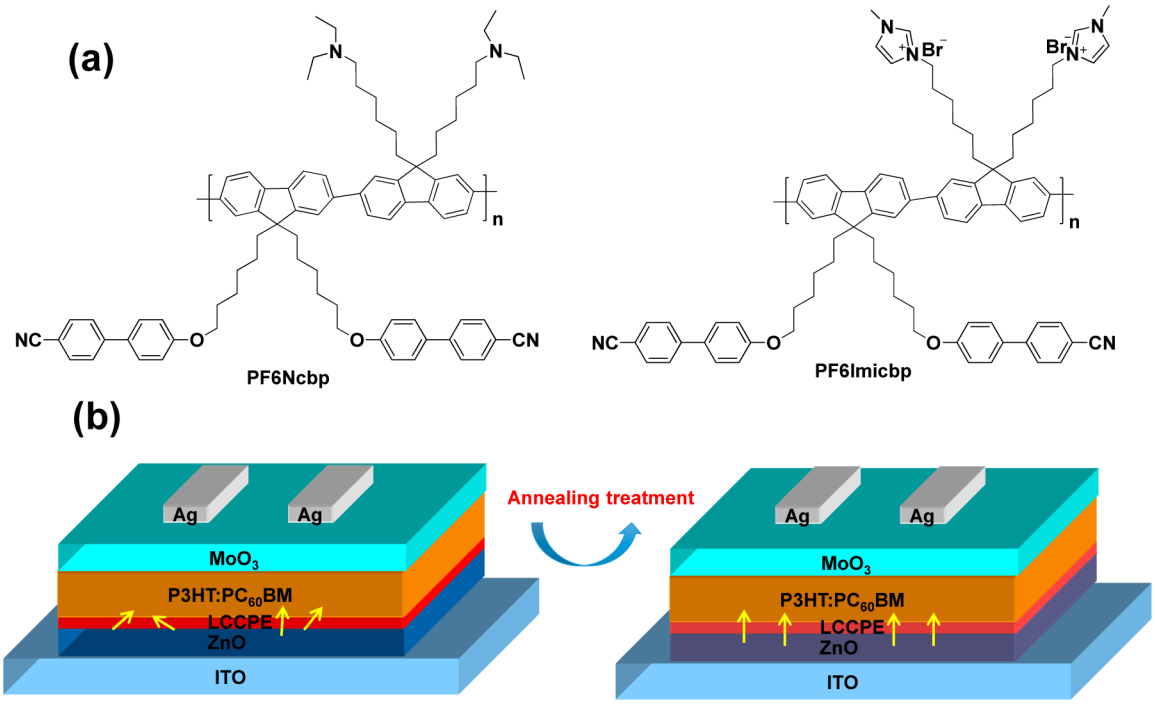

Figure 1. (a) Chemical structures of the LCCPEs PF6Ncbp and PF6Imicbp (b) i-PSC configuration and schematic representation of the reorientation of ZnO/LCCPE ETLs annealed at 150 °C for 10 min (the yellow arrows mean the direction of the dipoles).

carbonate (Cs_2CO_3)[12] are usually used as electron transport layer (ETL) to modulate the high work function of ITO and facilitate electron transportation. Among the aforementioned electron transport layer, ZnO is a promising candidate on account of relatively high electron mobility, optical transparency, and low work function, as well as its ease of fabrication.[13,14] However, the major challenges in using ZnO as ETLs are the existence of defects with adsorbed oxygen[15,16] and the incompatibility with upper organic active layer.In addition, the energy barrier still exist between ZnO ETL and electron acceptor in the inverted PSCs.[17,18] To passivate the surficial defects of ZnO, circumvent incompatible chemical interface and the unfavorable energetics, a series of novel organic interfacial materials such as ionic liquid materials,[19] self-assembled monolayer,[20] and fullerene derivatives[5,21,22] have been introduced to modify the ZnO buffer layer.

Recently, conjugated polyelectrolytes (CPEs) which feature a delocalized $\pi-\pi$ conjugated main backbone with pendant ionic groups on the side chains have emerged as notable modified interlayer of ZnO.[23,24] The CPEs are proved to help to establish a better contact between inorganic metal ZnO and organic layer in PSCs.[23,25] Moreover, they also facilitate charge transportation and collection by forming permanent dipole moments at the metal−organic interfaces, which has been inferred by reason for a spontaneous orientation of the ionic groups.[26−28]

Since the dipoles of CPE layer are determined by the spontaneous orientation of the ionic chains, more aligned dipoles can be achieved by introduction of ionic liquid crystal (ILC) into conjugated polyelectrolyte to form CPE-ILC complex.[29,30] The orientation of dipole moments at cathode interface was found to notably reduce the work function of ITO. As a result, a greatly improved device performance has been successfully achieved. Nevertheless, the ILC linked to CPE was not so robust through electrostatic attraction. In addition, the generated salts during the formation of CPE-ILC complex between CPE and ILC need to be completely removed, otherwise, the device efficiency may be devastated. To obtain more robust LC materials and alleviate the salt problem, two novel liquid-crystal conjugated polyelectrolytes (LCCPEs) poly[9,9-bis[6-(4-cyanobiphenyloxy)-hexyl]−fluorene−*alt*-9,9-bis(6-(N,N-diethylamino)-hexyl)-fluorene] (PF6Ncbp) and poly[9,9-bis[6-(4-cyano−biphenyloxy)-hexyl]−fluorene-*alt*-9,9-bis(6-(*N*-methylimidazole)-hexyl]-fluorene] (PF6Imicbp) are designed and synthesized by covalent linkage of the cyanobiphenyl mesogen polar groups onto conjugated polymers, rather than formation of the CPE-ILC complex. By this way, the orientation of dipoles can be successfully improved without interference with byproduct salts. CPEs contained with liquid-crystal group are further employed to modify ZnO ETL to boost the internal cell parameters of devices based on P3HT: $PC_{60}BM$ system. Meanwhile, to investigate the function of the cyanobiphenyl mesogens, poly[(9,9-bis(3′-(*N*,*N*-dimethylamino)-propyl)-2,7-fluorene)-*alt*-2,7-(9,9-dioctylfluorene)] (PFN) is chosen as a reference interlayer, which is analogous to PF6Ncbp but without liquid crystalline group on the side chains. It can be found that the introduction of mesogen groups and polar groups can endow conjugated polymer with mesomorphic properties[31,32] and good solubility in environmentally friendly solvents. More importantly, due to aligned dipoles induced by mesogen groups, compared with bare ZnO and PFN modified ZnO, the addition of LCCPEs PF6Ncbp and PF6Imicbp on ZnO film as ETL has remarkably improved the efficiency from 3.1% to 3.9% and 4.2%, respectively. These findings demonstrate that liquid-crystal conjugated polyelectrolytes are promising candidates to fabricate high effective polymer solar cells.

DOI: 10.1021/acsami.5b03340
ACS Appl. Mater. Interfaces 2015, 7, 19024−19033

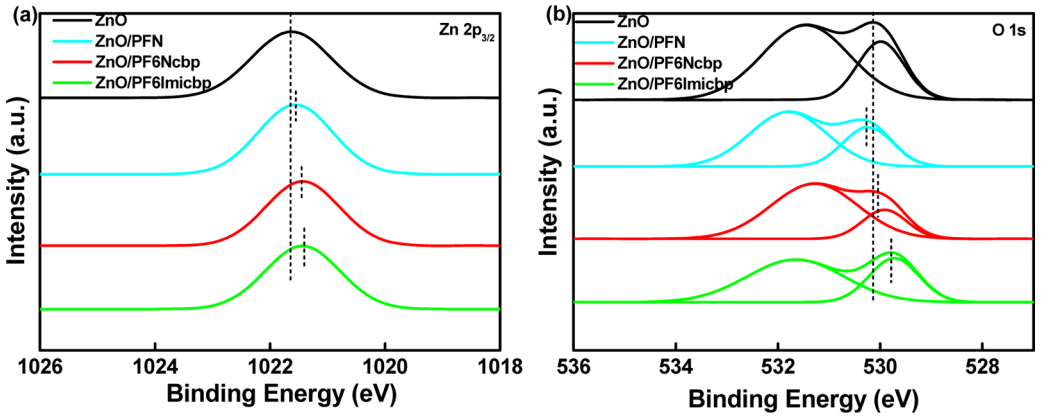

Figure 2. (a) High-resolution XPS of Zn $2p_{3/2}$ and (b) O 1s on the surface of ZnO, ZnO/PFN, ZnO/PF6Ncbp, and ZnO/PF6lmicbp on ITO substrates.

2. EXPERIMENTAL SECTION

2.1. Materials. all of the solvent and reagent were used as received. 2,7-dibromo-9,9-bis[6-(4′-cyanobiphenyloxy)-hexyl]−fluorene (F6Brcbp), 2,7-bis(4,4,5,5-tetramethyl[1,3,2]-dioxaborolan-2-yl)-9,9-bis(6-(4′-cyano-biphenyloxy)-hexyl]-fluorene (MBcbp), 2,7-dibromo-9,9-bis(6″(*N*,*N*-diethylamino)-hexyl)-fluorene (F6N) and 2,7-dibromo-9,9-bis(6-(*N*-methylimidazole)-hexyl]-fluorene (F6lmi) were synthesized according to the procedure reported by the literatures.[33−36]

2.2. Synthesis of the LCCPEs. The synthetic routes toward the target LCCPEs were outlined in Scheme S1. 2,7-Bis(4,4,5,5-tetramethyl[1,3,2]−dioxaborolan-2-yl)-9,9-bis(6-(4′-cyanobiphenyloxy)-hexyl]-fluorene (MBcbp) (0.35 mmol, 329 mg,) with 2,7-dibromo-9,9-bis(6″(*N*,*N*-diethylamino)-hexyl)-fluorene (F6N) (0.35 mmol, 221.3 mg,) and 2,7-dibromo-9,9-bis(6-(*N*-methylimidazole)-hexyl]-fluorene (F6lmi) (0.35 mmol, 225 mg,) by Suzuki coupling reaction at the presence of a few drops of methyl trioctyl ammonium chloride (Aliquat 336), 2 mL of 2 M Na_2CO_3 aqueous solution, tetrakis (triphenylphosphine) palladium [$(PPh_3)_4Pd(0)$] (20 mg), and chlorobenzene (7 mL) to obtain polymer PF6Ncbp and PF6lmicbp, respectively. The synthetic details and characterizations have been presented in the Supporting Information.

2.3. Device Fabrication. The ZnO precursor solution was obtained through dissolving ethanolamine ($NH_2CH_2CH_2OH$, 99.5%, 0.28 g), ethanolamine ($NH_2CH_2CH_2OH$, 99.5%, 0.28 g), and dihydrate ($Zn(CH_3COO)_2{\cdot}2H_2O$, 99.9%, 1 g) in 2-methoxyethanol ($CH_3OCH2CH_2OH$, 99.8%, 10 mL), with vigorous stirring overnight in air. All the solar cells were fabricated on previously cleaned ITO-coated glass substrates. All the ITO substrates were treated by UV ozone for 20 min. The ZnO precursor solution was spin-coated at 4000 rpm/min on surface of the ITO-glass substrates. The ITO substrate were by thermal annealing at 220 °C for 1 h in air. Subsequently, the ZnO film was covered with 0.25 mg/mL of CPE solution solved in methanol at 4000 rpm/min, then annealed at 150 °C for 10 min. The thickness of CPE was ca. 5 nm. The P3HT:PC_{60}BM blend system was prepared by dissolving P3HT (20 mg/mL) and PC_{60}BM (20 mg/mL) in 1 mL of ortho-dichlorobenzene. The P3HT:PC_{60}BM blend was spun-coat to form a 120 nm thin film. Heating treatment was taken by placing these samples on the heating stage at 150 °C for 10 min in a glovebox. The PTB7/PC_{70}BM system (1:1.5 by weight) was spun-coat from a chlorobenzene solution (25 mg/mL) with 3 vol % 1,8-diiodooctane as cosolvent at a speed of 1000 rpm/2 min. Finally, a 7 nm-thick MoO_3 and a 90 nm-thick Ag electrode was sequentially deposited by thermal evaporation.

3. RESULTS AND DISCUSSION

Figure 1a presents the chemical structures of the two liquid-crystal conjugated polyelectrolytes (LCCPEs). The structures of the two LCCPEs have been confirmed by NMR (Figure S1) and FT-IR (Figure S2). The cyano of cyanobiphenyl mesogens can be clearly detected by the peak stretching at 2224 cm^{-1} as revealed by the FT-IR spectra, indicating the successful incorporation of cyanobiphenyl mesogens into the polymers. The polymers PF6Ncbp and PF6lmicbp are easily dissolved in polar solvents, including dimethylformamide, dimethyl sulfoxide, environmentally friendly solvents alcohol and methanol, etc. PF6lmicbp can also be dissolved in water particularly, because of the imidazolium on the side chains. Through the gel permeation chromatograph (GPC), the molecular weights (M_n and M_w) and polydispersity index (PDI) of PF6Ncbp were 35.8, 64.4, and 1.8 kg mol^{-1}, respectively; PF6lmicbp were 33.6 and 50.4 kg mol^{-1}, respectively, polydispersity index (PDI) and 1.5. The thermostability of the copolymers was studied by thermogravimetric analysis (TGA) under a nitrogen atmosphere. The polymers PF6Ncbp and PF6lmicbp exhibited good thermostability with 5% loss at 235 and 262 °C, respectively (Figure S3). The mesomorphic behavior of the monomer MBcbp bearing mesogen groups, polymer PF6Ncbp and PF6lmicbp were studied by differential scanning calorimetry (DSC) (Figure S4a) and polarized optical microscope (POM) (Figure S4b). Because of the existence of the cyanobiphenyl mesogens, the monomer and corresponding polymers show liquid-crystalline optical anisotropy after thermal treatment. Compared with PF6Ncbp, PF6lmicbp with imidazolium group delivers brighter liquid crystalline texture, suggesting the more ordered packing in the polymer.[37] Combination of POM and DSC observation, PF6Ncbp and PF6lmicbp display liquid crystalline state to isotropic transition at 165.1 and 170.5 °C in the second heating circle, respectively. The optimized annealing temperature of 150 °C for P3HT:PC_{60}BM-based device is exactly located in the liquid crystalline temperature ranges of the two polymers, therefore, all of the samples and devices are annealed at 150 °C.

To explore the molecular interactions between the LCCPEs and ZnO, and whether the LCCPEs can passivate the defects of ZnO, the X-ray photoelectron spectroscopy (XPS) and photoluminescence (PL) measurements were carried out to confirm the PF6Ncbp and PF6lmicbp film deposited on ZnO. For comparison, the ZnO/PFN film was also prepared. High-resolution XPS spectra are shown in Figure S5a−c. The characteristic peak (N 1s) assigned to nitrogen portion in the PFN, PF6Ncbp and PF6lmicbp are clearly detected from the CPE-coated ZnO film samples at approximate 400 eV, indicating the successful deposition of CPE layers on the surface of the ZnO. Moreover, from the Figure 2a and b, it is

DOI: 10.1021/acsami.5b03340
ACS Appl. Mater. Interfaces 2015, 7, 19024−19033

found that O 1s and Zn $2p_{3/2}$ peaks are shifted after incorporation of the CPEs. Compared to the peak at 1021.64 eV which is related to the Zn $2p_{3/2}$ peak in the bare ZnO, the ZnO/PFN, ZnO/PF6Ncbp and ZnO/PF6lmicbp films show a Zn $2p_{3/2}$ peak at 1021.54, 1021.45, and 1021.42 eV by 0.10, 0.19, and 0.22 eV core level shift toward the lower binding energy, respectively. The down shift binding energy, especially in PF6Ncbp and PF6lmicbp modified ZnO, implies the more Zn atoms bounded to O atoms and the stronger intermolecular interaction between the LCCPEs and ZnO.[38] Similarly, the peak at 530.15 eV (assigned to O atoms presented in the bare ZnO matrix)[39] shifts to the lower blinding energy at 530.06 eV for ZnO/PF6Ncbp and 529.80 eV for ZnO/PF6lmicbp. However, the O 1s peak of PFN shifts to the higher blinding energy at 530.26 eV. The shifts to the lower binding energy may be attributed to the higher negative electric charge density on oxygen atoms owing to the electrostatic interaction (Figure 2b). To further verify the influence of CPEs modification on surface defects of ZnO, the photoelectricity of CPEs deposited on top of ZnO was measured by photoluminescence (PL) (Figure S6). Compared to the bare ZnO and ZnO/PFN with the surface defects emission at 450−550 nm, the intensity of defect emission is considerably restrained after incorporation of LCCPEs on ZnO. The reduction of traps could decrease the possibility of bimolecular recombination of the device,[40] consequently contributing to an improvement of fill factor (FF) and a short-circuit current density (J_{sc}).

In consideration of the apparent shift in Zn $2p_{3/2}$ and O 1s XPS peaks of LCCPEs modified ZnO, the energy states of ZnO/LCCPEs are expected to be re-engineered.

The change of the binding-energy of the ZnO/LCCPEs films was studied by Ultraviolet photoelectron spectroscopy (UPS). The HOMO energies are determined in line with the following equation[41]

$$\text{HOMO} = h\nu - (E_{\text{cutoff}} - E_{\text{onset}})$$

where $h\nu$ is the incident photon energy ($h\nu$ = 21.2 eV) for He I. The related spectra and data are presented in Figure 3a and Table 1. In Figure 3a, the high binding-energy cutoff (E_{cutoff}) of ZnO, ZnO/PFN, ZnO/PF6Ncbp, and ZnO/PF6lmicbp are 14.35, 14.85, 15.03, and 15.08 eV, respectively, and E_{onset} that is generally referred as the binding energy onset, is 0.90 eV for bare ZnO, 1.06 eV for ZnO/PFN, 1.06 eV for ZnO/PF6Ncbp, and 1.08 eV for ZnO/PF6lmicbp. The incident photon energy $h\nu$ is 21.22 eV, so the estimated HOMO energy is −7.77 eV for ZnO, −7.43 eV for ZnO/PFN, −7.25 eV for ZnO/PF6Ncbp, and −7.22 eV for ZnO/PF6lmicbp. On the basis of these HOMO energies and optical gaps determined by the ultraviolet−visible (UV−vis) absorption spectra (see Figure S7), the calculated LUMO energy levels of ZnO, ZnO/PFN, ZnO/PF6Ncbp, and ZnO/PF6lmicbp are −4.49, −4.15, −3.97, and −3.92 eV, respectively. The optical gap of ZnO and ZnO/CPE are calculated through the equation[42]

$$(\alpha h\nu)^2 = A(h\nu - E_g)$$

where A is a constant and α is the extinction coefficient of ZnO. An energy-level figure is constructed to visually expound the shift of the energy levels in Figure 3b. The shifts in LUMO energies levels demonstrate that the LUMO energy levels of ZnO are well re-engineered by insertion of a thin layer of LCCPEs, sequentially yielding a preferable LUMO energy alignment at the ZnO-active layer interface which is in favor of

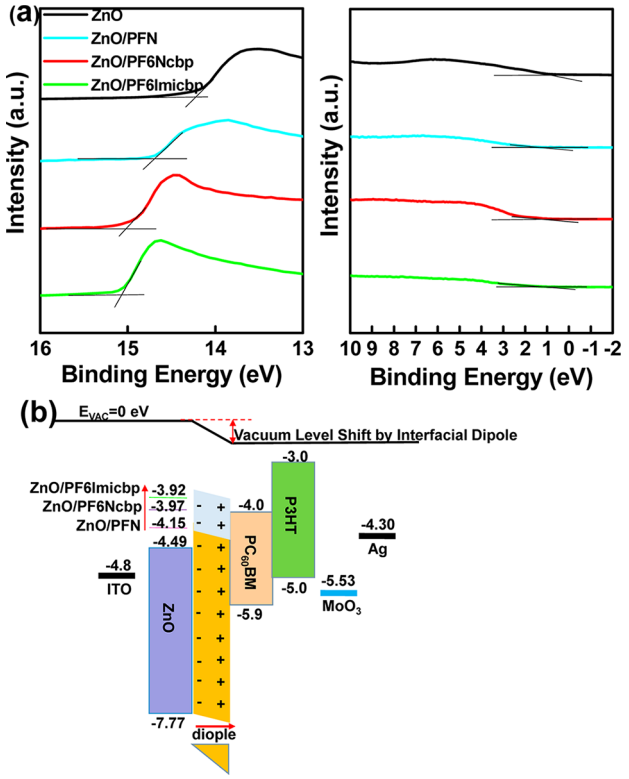

Figure 3. (a) UPS results of of ZnO, ZnO/PFN, ZnO/PF6Ncbp and ZnO/PF6lmicbp ETLs with (left) the high binding energy cutoff and (right) the HOMO region. (b) Schematic energy-level diagram of each component material based on P3HT:$PC_{60}BM$ device.

Table 1. Energy Levels of the ZnO and ZnO/CPEs

ETL	E_g (eV)	E_{cutoff} (eV)	E_{onset} (eV)	HOMO (eV)	LUMO (eV)
ZnO	3.28	14.35	0.90	−7.77	−4.49
ZnO/PFN	3.28	14.85	1.06	−7.43	−4.15
ZnO/PF6Ncbp	3.28	15.03	1.06	−7.25	−3.97
ZnO/ PF6lmicbp	3.28	15.08	1.08	−7.22	−3.92

the electron transfer and collection. The shift of energy between ZnO and ZnO/CPE bilayers demonstrate that interfacial dipoles are generated between the ZnO layer and CPEs.[24] Although the structures of PFN and PF6Ncbp only differ with the functional groups, the binding-energy of PF6Ncbp shifts to the lower level. The result can be explained by that the ordered polar chains induced by the liquid crystal are preferable to form an aligned dipole moment, promoting a better energy alignment at the ZnO/$PC_{60}BM$ interface.[30] In addition, the lower LUMO energy of ZnO/PF6lmicbp than that of ZnO/PF6Ncbp results from the stronger electronic interaction at ZnO/PF6lmicbp interface than that at ZnO/PF6Ncbp interface, as observed by XPS.

Water contact angel measurement was used to investigate the surface property of the ZnO/LCCPEs bilayers. Seen from Figure 4, obvious changes of water contact angle on the surface of ZnO/PF6Ncbp and ZnO/PF6lmicbp could be observed before and after annealing at 150 °C for 10 min. The water contact angels of PF6Ncbp and PF6lmicbp increase from 79° to 89° and from 44° to 52°, respectively, which reveal that the hydrophobicity of ZnO/LCCPEs bilayers are remarkably improved. However, for the ZnO/PFN, thermal treatment

DOI: 10.1021/acsami.5b03340
ACS Appl. Mater. Interfaces 2015, 7, 19024−19033

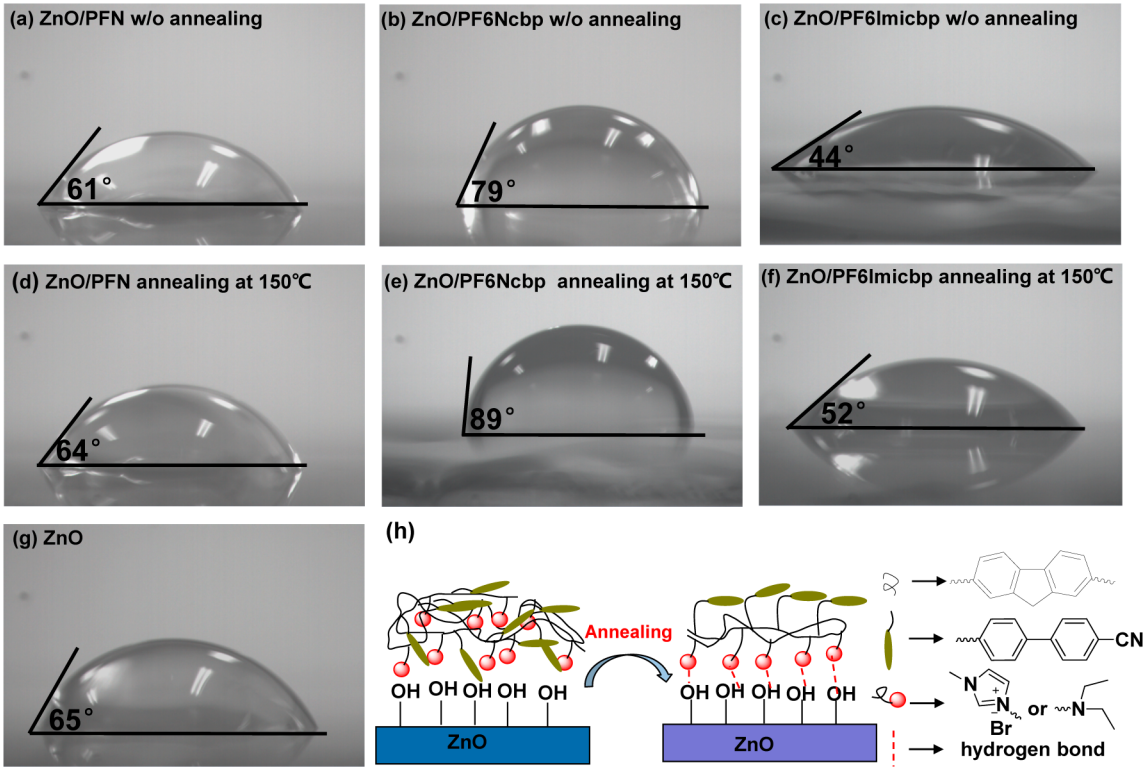

Figure 4. Water contact angle images of (a, d) ZnO/PF6Ncbp, (b, e) ZnO/PF6Imicbp, (c, f) ZnO/PFN, and (g) ZnO films without or with thermal treatment at 150 °C for 10 min. (h) The schematic illustration of the orientation of the mesomorphic groups after thermal treatment at 150 °C for 10 min.

only slightly increases the water contact angle from 61° to 64°. The increased water contact angle of the ZnO/PFN upon thermal annealing should be attributed to the rearrangement of hydrophobic conjugated polymer backbone at the surface. After incorporation of the mesogen groups into the CPEs, the spontaneous orientation of the hydrophobic mesomorphic moieties would further induce the hydrophobic moieties to preferentially be located on the film surface,[43] while the polar groups tend to be located near the hydrophilic ZnO, as schematically illustrated in Figure 4h. The substantially improved hydrophobicity of the ZnO/LCCPEs could form a more intimate interfacial contact with upper photon harvesting layer than PFN, in favor of the charge injection and collection.

Since the orientation of the incorporated mesogen groups can induce a rearrangement of the LCCPEs on the ZnO surface, such morphology change may cause a distinct change on the upper active layer. Figure S8 demonstrates the surface morphologies of modified ZnO studied by the atomic force microscopy (AFM). With a scale of 5 μm × 5 μm, the root-mean-square (rms) of bare ZnO, ZnO/PFN6cbp, and ZnO/PF6Imicbp are 1.23, 1.30, and 6.87 nm, respectively. Deposition of the P3HT:$PC_{60}BM$ on these interfacial layers results in a smooth surface with a rms of 0.96 nm for bare ZnO, 1.08 nm for ZnO/PFN6cbp, and 1.76 nm for ZnO/PF6Imicbp. Except the increased roughness, distinct morphology change, especially after deposition on ZnO/PF6Imicbp, can also be observed by AFM images, indicating that LCCPEs offer enhanced interfacial adhesion interaction.[44] In addition, the LCCPEs show more homogeneous morphology than the CPE-ILC complex, for the salts problem has been avoided.[30] The evidence of improved morphology in the blend can also be supported by transmission electron microscopy (TEM), as displayed in Figure 5.

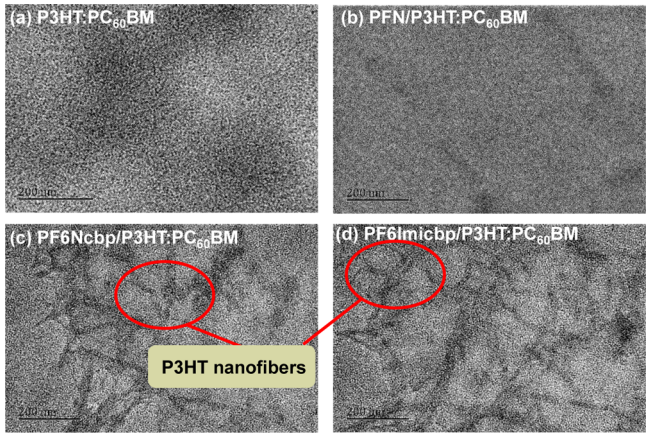

Figure 5. TEM images of P3HT:$PC_{60}BM$ films on top of the (a) ZnO, (b) ZnO/PFN, (c) ZnO/PF6Ncbp, and (d) ZnO/PF6Imicbp layers after thermal treatment at 150 °C for 10 min.

Compared with P3HT:$PC_{60}BM$ deposited on bare ZnO and ZnO/PFN in Figure 5a and b, incorporation of mesomorphic conjugated polyelectrolytes interlayers lead to a significant change in the P3HT:$PC_{60}BM$ morphology. In Figure 5c and d, a large amount of nanofibers emerge in the P3HT:$PC_{60}BM$ blend, since that the well-organized of thermotropic liquid crystalline CPEs after the thermal annealing can serve as a structural template for the molecular orientation of P3HT. These nanofibers in the active layer are very favorable for charge transport. The ordered morphology can be further verified by the UV−Vis absorption spectra. As shown in Figure S9, all of P3HT:$PC_{60}BM$ show a shoulder peak at about 600 nm, ascribing to the characteristic peaks of the crystalline

DOI: 10.1021/acsami.5b03340
ACS Appl. Mater. Interfaces 2015, 7, 19024−19033

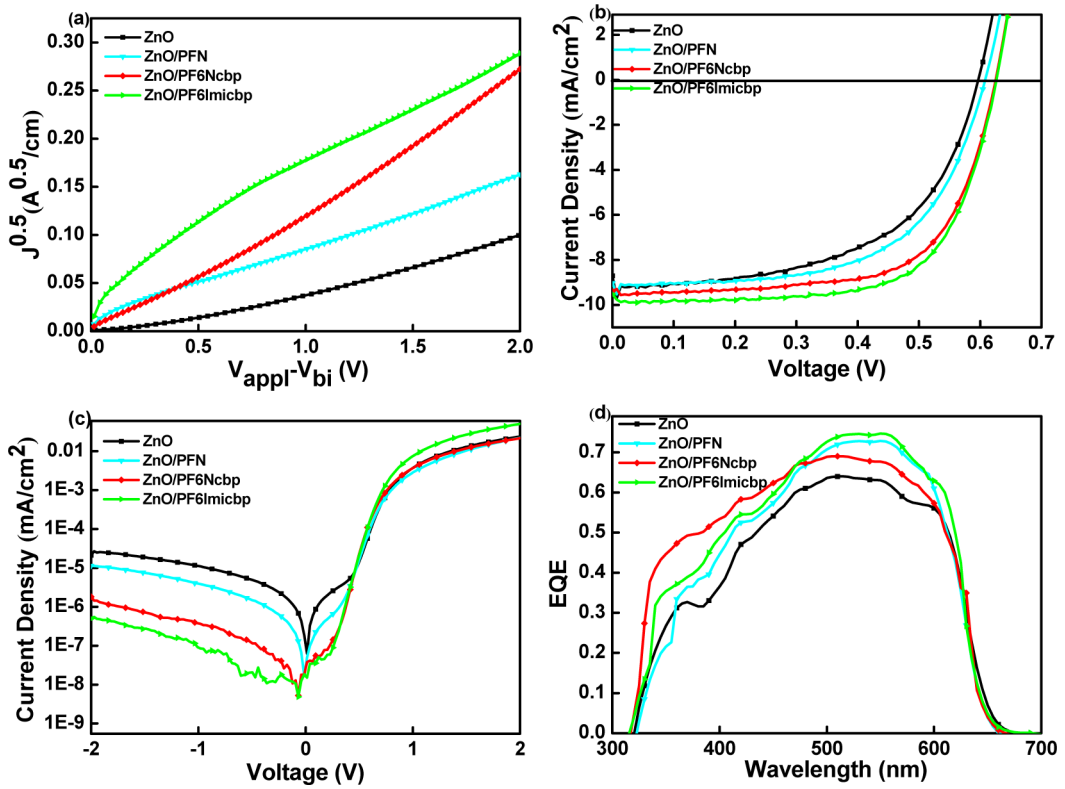

Figure 6. (a) $J^{0.5}-V$ characteristics of electron-only devices with ZnO and ZnO/CPE bilayers. (b) $J-V$ characteristics, (c) dark current of the i-PSCs with ZnO and ZnO/CPE bilayers, and (d) EQE characteristics.

P3HT.[45] Compared with the bare ZnO and ZnO/PFN, LCCPEs induce an obviously enhancement in intensity of 605 nm after magnified, indicating that the crystallization of P3HT chains are really enhanced by the mesomorphic moieties. The improved morphology of the active layer promoted by LCCPEs can facilitate the charge transfer and transport. As observed by photoluminescence spectra of P3HT:$PC_{60}BM$ blends on different ETLs in Figure S10, PL quenching after incorporation of LCCPEs are more obvious than that of PFN, meaning that more efficient charge transfer occurred between liquid-crystal CPEs and active layer.

Charge carrier mobility is also one of crucial parameters in the design of interfacial materials for highly efficient photovoltaic solar cells. To explore the electron transfer characteristic of ZnO ETL and ZnO/CPEs ETL, the electron transport characteristics was measured by the space charge limited current (SCLC) model according to the Mott−Gurney equations[46−49] (the details of the mobility measurement are described in the Supporting Information). With respect to the electron mobility of bare ZnO ETLs (9.85×10^{-5} cm^2 V^{-1} s^{-1}) (Figure 6a and Table 2), the devices with ZnO/PF6Ncbp and ZnO/PF6Imicbp ensure an apparent increase to 4.13×10^{-4} and to 4.9×10^{-4} cm^2 V^{-1} s^{-1}, respectively, even higher than that of ZnO/PFN (1.43×10^{-4} cm^2 V^{-1} s^{-1}). The improvement of electron mobilities can be correlated to the ordered morphology of the interfacial layer, the enhancement of the crystallinity of the active layer and the imitate contact between interfacial layer and active layer.

Table 2. Electron Mobility Based on P3HT:$PC_{60}BM$ Device with Various ETLs

ETL	electron mobility (cm^2/v·s)
ZnO	9.85×10^{-5}
ZnO/PFN	1.43×10^{-4}
ZnO/PF6Ncbp	4.13×10^{-4}
ZnO/PF6Imicbp	4.9×10^{-4}

The optical transmittance spectra of ZnO/LCCPE ETLs were investigated as presented in Figure S11, the optical absorption of these ZnO/CPE bilayers are marginally different to that of bare ZnO, suggesting that these modification layers would not hinder the light-absorption of active layer. To explore the impacts on photovoltaic characteristics after deposition the LCCPEs on ZnO, the inverted organic solar cells based on polyelectrolyte-coated ZnO bilayers were fabricated with the ITO/ZnO/CPE/P3HT:$PC_{60}BM$/MoO_3/Ag, as shown in Figure 1b. Figure 6b presented the current density−voltage ($J-V$) characteristics of the inverted PSCs based on P3HT:$PC_{60}BM$ system under AM 1.5 G illumination at 100 mW/cm^2, and the related device parameters are presented in Table 3. The device with bare ZnO layer exhibits the lowest PCE of 3.1% with an open-circuit voltage (V_{oc}) of 0.60 V, J_{sc} of 8.88 mA cm^{-2}, and FF of 59.6%, in accordance with the reported value.[50] After deposition of an additional PFN on ZnO, the PCE of the device is slightly improved to 3.3%. Intriguingly, the PCEs of the devices for liquid-crystal polyelectrolytes PF6Ncbp and PF6Imicbp are dramatically improved to 3.9% and 4.2%, respectively. The optimized device efficiency by insertion of LCCPEs as modified layers is related to the overall enhanced device parameters, including V_{oc}, J_{sc}, and FF. The better energy alignment created by the LCCPEs should be responsible for the V_{oc} and J_{sc} enhancement, as supported by UPS. In addition, the favorable morphology of the interfacial layer and active layer, improved interfacial

DOI: 10.1021/acsami.5b03340
ACS Appl. Mater. Interfaces 2015, 7, 19024−19033

Table 3. Devices Performance Based on P3HT:$PC_{60}BM$ Solar Cells with Various Interlayers[a]

ETL	V_{oc} (V)	J_{sc}[b] (mA/cm^2)	FF (%)	PCE (%)
ZnO	0.600 ± 0.010	8.88 ± 0.82 (8.55)[c]	59.6 ± 3.1	3.1 ± 0.3
ZnO/PFN	0.608 ± 0.010	9.02 ± 0.73 (9.00)[c]	60.5 ± 2.2	3.3 ± 0.2
ZnO/PF6Ncbp	0.624 ± 0.020	9.39 ± 0.81 (9.30)[c]	66.7 ± 1.8	3.9 ± 0.2
ZnO/PF6lmicbp	0.626 ± 0.020	9.52 ± 0.74 (9.45)[c]	69.8 ± 2.1	4.2 ± 0.2

[a]Composition of photovoltaic device: ITO/ETL/P3HT:$PC_{60}BM$ (120 nm)/MoO_3 (7 nm)/Ag (90 nm). [b]The J_{sc} values were estimated from the measured active area. [c]J_{sc} values estimated through EQE data in Figure 6d. The device parameters showed the average values of 10 cells of each BHJ type.

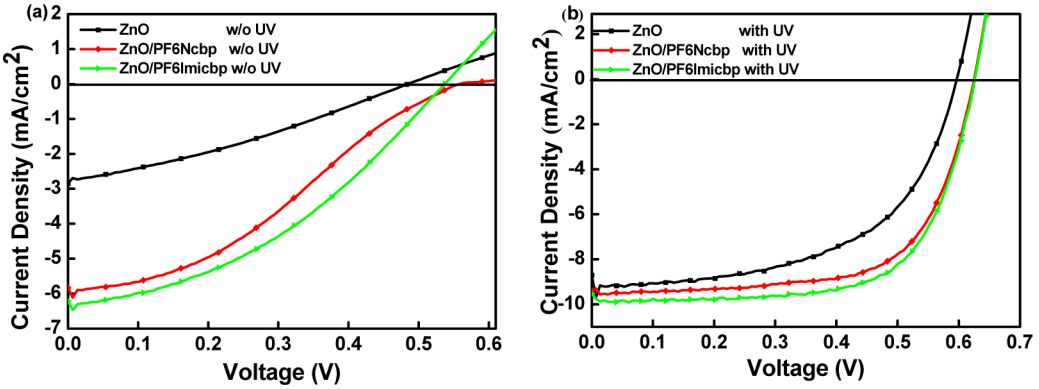

Figure 7. $J-V$ curves of devices based on P3HT:$PC_{60}BM$ with various interlayers under AM1.5 illumination (100 mW/cm^2) without (a) and with (b) UV block filter.

compatibility, and faster electron mobility also contribute to the increasement in J_{sc} and FF. From the Figure 6b and Table 3, we can see that, compared with PF6Ncbp modified ZnO, ZnO/PF6lmicbp shows superior interfacial modification and obtains the higher efficiency. The outstanding performance of ZnO/PF6lmicbp mainly originates from stronger interaction with ZnO and more efficient charge transfer in the active layer, as reveal by the more PL quenching (Figure S10). As a comparison, LCCPEs were applied to modify the ITO cathode. As displayed in Figure S12 and Table S1, the best PCE among all devices was below 2.5%, which was imputed to the poor FF and J_{sc}.

The dark $J-V$ characteristics were investigated to further evaluate the electrical characteristics of the ZnO/CPE interlayers in inverted devices. As shown Figure 6c, it clearly find that the dark current densities of ZnO/PF6Ncbp and ZnO/PF6lmicbp interfacial layer under the reverse bias are approximately 10 times smaller than those with ZnO/PFN and bare ZnO interfacial layers. And the leakage current of ZnO/PF6lmicbp is lower than that of ZnO/PF6Ncbp under the reverse bias, meaning that utilizing PF6lmicbp as modification layer results in a more efficient suppression of excitons recombination.[51,52] To further verify the accuracy of J_{sc} obtained by from $J-V$ characteristic curve, the external quantum efficiencies (EQE) of i-PSCs based on ZnO, ZnO/PFN, ZnO/PF6Ncbp, and ZnO/PF6lmicbp were measured, shown in Figure 6d. All J_{sc} values calculated by EQE are quite in consistent with the values achieved from $J-V$ curves. Moreover, compared to the device with bare ZnO, the ones with LCCPEs, especially with PF6Ncbp showed much higher EQE from 300 to 400 nm, which also contribute to the J_{sc} enhancement.

As known that ZnO electron extraction layers suffered from the "light-soaking" issue, which meant that the device incorporated with ZnO exposured with UV light could enhance device performance.[53] In order to check whether the "light-soaking" issue could be solved by the usage of LCCPE, the as prepared devices were measured with the AM1.5 simulated sun light applying a UV blocking filter to block all wavelengths shorter than 390 nm. The results were shown in the Figure 7a, the devices showed nonideal characteristics with a low FF and a low PCE. However, the phenomenon could be solved by exposing to UV illumination as seen in Figure 7b. Thus, UV exposure was required to acquire an ideal device characteristics with a high FF and an excellent PCE.[53,54]

To verify the universal validity of the LCCPEs on common PSCs, inverted polymer–fullerene PSCs based on the lowband gap polymer PTB7 with ZnO/LCCPE were fabricated by the ITO/ZnO/LCCPE/PTB7:$PC_{70}BM$/MoO_3/Ag structure. The $J-V$ curves and the related device parameters were presented in Figure 8 and Table 4. As expected, the average efficiency of the devices boost sharply from 6.4% for bare ZnO to 7.2% for ZnO/PF6Ncbp and 7.6% for ZnO/PF6lmicbp with the

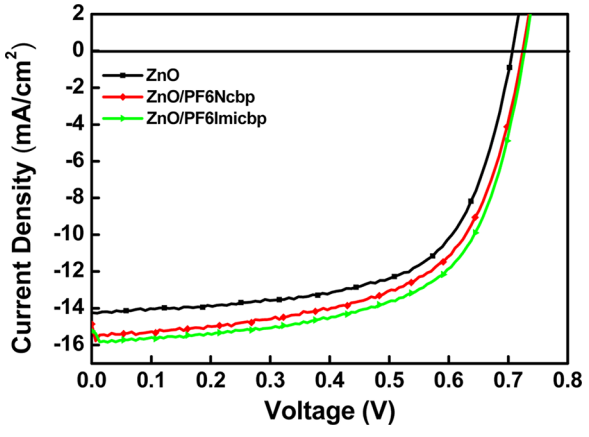

Figure 8. $J-V$ curves of devices based on PTB7:$PC_{70}BM$ with various interlayers.

DOI: 10.1021/acsami.5b03340
ACS Appl. Mater. Interfaces 2015, 7, 19024–19033

Table 4. Devices Performance Based on PTB7:$PC_{70}BM$ Solar Cells with Various Interlayers[a]

ETL	V_{oc} (V)	J_{sc}[b] (mA/cm^2)	FF (%)	PCE (%)
ZnO	0.706 ± 0.020	14.25 ± 0.65 (13.85)[c]	63.7 ± 1.12	6.4 ± 0.30
ZnO/PF6Ncbp	0.724 ± 0.010	15.64 ± 0.73 (15.34)[c]	63.6 ± 1.90	7.2 ± 0.51
ZnO/PF6lmicbp	0.727 ± 0.010	16.03 ± 0.82 (15.76)[c]	64.9 ± 1.75	7.6 ± 0.42

[a]Composition of photovoltaic device: ITO/ETL/PTB7:$PC_{70}BM$/MoO_3 (7 nm)/Ag (90 nm). [b]The J_{sc} values were estimated from the measured active area. [c]J_{sc} values estimated through EQE data in Figure S13. The device parameters showed the average values of 10 cells of each BHJ type.

enhancement of J_{sc} and V_{oc}. Compared to the control devices with bare ZnO exhibiting a J_{sc} of 14.25 mA/cm^2, a V_{oc} of 0.706 V, the ZnO/PF6Ncbp and ZnO/PF6lmicbp achieved a J_{sc} of 15.64 mA/cm^2 and 16.03 mA/cm^2, a V_{oc} of 0.724 and 0.727 V, respectively. The EQE spectra of the devices were displayed in Figure S13. Therefore, liquid-crystal conjugated polyelectrolytes showed the general applicability to fabricate high efficiency organic polymer cells.

4. CONCLUSIONS

To summarize, we have successfully designed and synthesized water/alcohol soluble LCCPEs PF6Ncbp and PF6lmicbp through covalent bond of liquid-crystal polar groups onto conjugated polyelectrolytes for ZnO modification. Compared with PFN without mesogenic groups, PF6Ncbp and PF6lmicbp not only can form a more aligned dipole moment to eliminate energy barrier, but also can induce the upper active layer to form better crystallization morphology, which facilitate the electron extraction and transportation. Significant enhancement of PCEs can be achieved by deposition of liquid-crystal polyelectrolytes PF6Ncbp and PF6lmicbp on ZnO as ETL. The outstanding performance of ZnO/PF6lmicbp than the ZnO/PF6Ncbp originates from the stronger interaction with ZnO and more efficient charge transfer in the active layer. Considering the two materials have merged the green solvent processability, excellent electron transportation ability and high efficiency together, LCCPEs are prospected to be promising candidates to apply in roll-to-roll manufacturing techniques for high performance devices.

■ ASSOCIATED CONTENT

Supporting Information

The Supporting Information is available free of charge on the ACS Publications website at DOI: 10.1021/acsami.5b03340.

Detailed experimental sections, the synthesis of the monomers and polymers, and the corresponding characterization (PDF)

■ AUTHOR INFORMATION

Corresponding Author

*Tel.: +86 791 83968703. Fax: +86 791 83968830. E-mail: chenlie@ncu.edu.cn.

Notes

The authors declare no competing financial interest.

■ ACKNOWLEDGMENTS

This work was financially supported by the National Science Fund for Distinguished Young Scholars (51425304), National Natural Science Foundation of China (51263016, 51473075 and 21402080), National Basic Research Program of China (973 Program 2014CB260409), and the Natural Science Foundation of Jiangxi Province (20143ACB20001 and 20151BAB203016).

■ REFERENCES

(1) Yu, G.; Gao, J.; Hummelen, J. C.; Wudl, F.; Heeger, A. J. Polymer Photovoltaic Cells: Enhanced Efficiencies via a Network of Internal Donor-acceptor Heterojunctions. *Science* **1995**, *270*, 1789−1791.

(2) Dennler, G.; Scharber, M. C.; Brabec, C. J. Polymer-fullerene Bulk-heterojunction Solar Cells. *Adv. Mater.* **2009**, *21*, 1323−1338.

(3) Li, G.; Zhu, R.; Yang, Y. Polymer Solar Cells. *Nat. Photonics* **2012**, *6*, 153−161.

(4) Li, C.-Y.; Wen, T.-C.; Lee, T.-H.; Guo, T.-F.; Huang, J.-C.-A.; Lin, Y.-C.; Hsu, Y.-J. An Inverted Polymer Photovoltaic Cell with Increased Air Stability Obtained by Employing Novel Hole/Electron Collecting Layers. *J. Mater. Chem.* **2009**, *19*, 1643−1647.

(5) Hsieh, C.-H.; Cheng, Y.-J.; Li, P.-J.; Chen, C.-H.; Dubosc, M.; Liang, R.-M.; Hsu, C.-S. Highly Efficient and Stable Inverted Polymer Solar Cells Integrated with a Cross-linked Fullerene Material as an Interlayer. *J. Am. Chem. Soc.* **2010**, *132*, 4887−4893.

(6) Xu, Z.; Chen, L.-M.; Yang, G.; Huang, C.-H.; Hou, J.; Wu, Y.; Li, G.; Hsu, C.-S.; Yang, Y. Vertical Phase Separation in Poly(3-hexylthiophene): Fullerene Derivative Blends and its Advantage for Inverted Structure Solar Cells. *Adv. Funct. Mater.* **2009**, *19*, 1227−1234.

(7) Jorgensen, M.; Norrman, K.; Gevorgyan, S. A.; Tromholt, T.; Andreasen, B.; Krebs, F. C. Stability of Polymer Solar Cells. *Adv. Mater.* **2012**, *24*, 580−612.

(8) Wang, W.; Schaffer, C. J.; Song, L.; Körstgens, V.; Pröller, S.; Indari, E. D.; Wang, T.; Abdelsamie, A.; Bernstorff, S.; Müller-Buschbaum, P. In Operando Morphology Investigation of Inverted Bulk Heterojunction Organic Solar Cells by GISAXS. *J. Mater. Chem. A* **2015**, *3*, 8324−8331.

(9) Yip, H.-L.; Jen, A. K. Y. Recent Advances in Solution-processed Interfacial Materials for Efficient and Stable Polymer Solar Cells. *Energy Environ. Sci.* **2012**, *5*, 5994.

(10) Hau, S. K.; Yip, H.-L.; Baek, N. S.; Zou, J.; O'Malley, K.; Jen, A. K. Y. Air-stable Inverted Flexible Polymer Solar Cells Using Zinc Oxide Nanoparticles as an Electron Selective Layer. *Appl. Phys. Lett.* **2008**, *92*, 253301.

(11) Hau, S. K.; Yip, H.-L.; Acton, O.; Baek, N. S.; Ma, H.; Jen, A. K. Y. Interfacial Modification to Improve Inverted Polymer Solar Cells. *J. Mater. Chem.* **2008**, *18*, 5113−5119.

(12) Li, G.; Chu, C. W.; Shrotriya, V.; Huang, J.; Yang, Y. Efficient Inverted Polymer Solar Cells. *Appl. Phys. Lett.* **2006**, *88*, 253503.

(13) Yan, H.; Lee, P.; Armstrong, N. R.; Graham, A.; Evmenenko, G. A.; Dutta, P.; Marks, T. J. High-performance Hole-Transport Layers for Polymer Light-emitting Diodes. Implementation of Organosiloxane Cross-linking Chemistry in Polymeric Electroluminescent Devices. *J. Am. Chem. Soc.* **2005**, *127*, 3172−3183.

(14) Jørgensen, M.; Norrman, K.; Krebs, F. C. Stability/Degradation of Polymer Solar Cells. *Sol. Energy Mater. Sol. Cells* **2008**, *92*, 686−714.

(15) Zhang, Y.; Du, G.; Wang, X.; Li, W.; Yang, X.; Ma, Y.; Zhao, B.; Yang, H.; Liu, D.; Yang, S. X-ray Photoelectron Spectroscopy Study of ZnO Films Grown by Metal-organic Chemical Vapor Deposition. *J. Cryst. Growth* **2003**, *252*, 180−183.

(16) Wei, X. Q.; Man, B. Y.; Liu, M.; Xue, C. S.; Zhuang, H. Z.; Yang, C. Blue Luminescent Centers and Microstructural Evaluation by XPS and Raman in ZnO Thin Films Annealed in Vacuum, N2 and O2. *Phys. B* **2007**, *388*, 145−152.

(17) Choi, H.; Park, J. S.; Jeong, E.; Kim, G. H.; Lee, B. R.; Kim, S. O.; Song, M. H.; Woo, H. Y.; Kim, J. Y. Combination of Titanium Oxide and a Conjugated Polyelectrolyte for High-performance

DOI: 10.1021/acsami.5b03340
ACS Appl. Mater. Interfaces 2015, 7, 19024−19033

Inverted-type Organic Optoelectronic Devices. *Adv. Mater.* **2011**, *23*, 2759−2763.
(18) Ma, H.; Yip, H.-L.; Huang, F.; Jen, A. K. Y. Interface Engineering for Organic Electronics. *Adv. Funct. Mater.* **2010**, *20*, 1371−1388.
(19) Lee, B. R.; Choi, H.; SunPark, J.; Lee, H. J.; Kim, S. O.; Kim, J. Y.; Song, M. H. Surface Modification of Metal Oxide Using Ionic Liquid Molecules in Hybrid Organic-inorganic Optoelectronic Devices. *J. Mater. Chem.* **2011**, *21*, 2051−2053.
(20) Bulliard, X.; Ihn, S.-G.; Yun, S.; Kim, Y.; Choi, D.; Choi, J.-Y.; Kim, M.; Sim, M.; Park, J.-H.; Choi, W.; Cho, K. Enhanced Performance in Polymer Solar Cells by Surface Energy Control. *Adv. Funct. Mater.* **2010**, *20*, 4381−4387.
(21) Cheng, Y.-J.; Hsieh, C.-H.; He, Y.; Hsu, C.-S.; Li, Y. Combination of Indene-C60 Bis-Adduct and Cross-linked Fullerene Interlayer Leading to Highly Efficient Inverted Polymer Solar Cells. *J. Am. Chem. Soc.* **2010**, *132*, 17381−17383.
(22) Li, P.; Li, X.; Sun, C.; Wang, G.; Li, J.; Jiu, T.; Fang, J. Performance Enhancement of Inverted Polymer Solar Cells with Fullerene Ester Derivant-modified ZnO Film as Cathode Buffer Layer. *Sol. Energy Mater. Sol. Cells* **2014**, *126*, 36−41.
(23) Yang, T.; Wang, M.; Duan, C.; Hu, X.; Huang, L.; Peng, J.; Huang, F.; Gong, X. Inverted Polymer Solar Cells with 8.4% Efficiency by Conjugated Polyelectrolyte. *Energy Environ. Sci.* **2012**, *5*, 8208−8214.
(24) Woo, S.; Hyun Kim, W.; Kim, H.; Yi, Y.; Lyu, H.-K.; Kim, Y. 8.9% Single-stack Inverted Polymer Solar Cells with Electron-rich Polymer Nanolayer-modified Inorganic Electron-collecting Buffer Layers. *Adv. Energy Mater.* **2014**, DOI: 10.1002/aenm.201301692.
(25) Choi, H.; Park, J. S.; Jeong, E.; Kim, G.-H.; Lee, B. R.; Kim, S. O.; Song, M. H.; Woo, H. Y.; Kim, J. Y. Combination of Titanium Oxide and a Conjugated Polyelectrolyte for High-performance Inverted-type Organic Optoelectronic Devices. *Adv. Mater.* **2011**, *23*, 2759−2763.
(26) Oh, S.-H.; Na, S.-I.; Jo, J.; Lim, B.; Vak, D.; Kim, D.-Y. Water-soluble Polyfluorenes as an Interfacial Layer Leading to Cathode-independent High Performance of Organic Solar Cells. *Adv. Funct. Mater.* **2010**, *20*, 1977−1983.
(27) He, Z.; Zhong, C.; Su, S.; Xu, M.; Wu, H.; Cao, Y. Enhanced Power-conversion Efficiency in Polymer Solar Cells Using an Inverted Device Structure. *Nat. Photonics* **2012**, *6*, 591−595.
(28) Zhong, Y.; Ma, J.; Hashimoto, K.; Tajima, K. Electric Field-induced Dipole Switching at the Donor/Acceptor Interface in Organic Solar Cells. *Adv. Mater.* **2013**, *25*, 1071−1075.
(29) Chen, L.; Xie, C.; Chen, Y. Optimization of the Power Conversion Efficiency of Room Temperature-fabricated Polymer Solar Cells Utilizing Solution Processed Tungsten Oxide and Conjugated Polyelectrolyte as Electrode Interlayer. *Adv. Funct. Mater.* **2014**, *24*, 3986−3995.
(30) Chen, L.; Xie, C.; Chen, Y. Self-assembled Conjugated Polyelectrolyte−ionic Liquid Crystal Complex as an Interlayer for Polymer Solar Cells: Achieving Performance Enhancement via Rapid Liquid Crystal-induced Dipole Orientation. *Macromolecules* **2014**, *47*, 1623−1632.
(31) Zhang, D.; Liu, Y.; Wan, X.; Zhou, Q.-F. Synthesis of a New Side-chain Type Liquid Crystal Polymer Poly[dicyclohexyl vinyl-terephthalate]. *Macromolecules* **1999**, *32*, 4494−4496.
(32) Goto, H.; Dai, X.; Ueoka, T.; Akagi, K. Synthesis and Properties of Polymers from Monosubstituted Acetylene Derivatives Bearing Ferroelectric Liquid Crystalline Groups. *Macromolecules* **2004**, *37*, 4783−4793.
(33) Jo, J.; Chi, C.; Hoger, S.; Wegner, G.; Yoon, D. Y. Synthesis and Characterization of Monodisperse Oligofluorenes. *Chem. - Eur. J.* **2004**, *10*, 2681−2688.
(34) Yao, K.; Chen, Y.; Chen, L.; Li, F.; Li, X.; Ren, X.; Wang, H.; Liu, T. Mesogens Mediated Self-assembly in Applications of Bulk Heterojunction Solar Cells Based on a Conjugated Polymer with Narrow Band Gap. *Macromolecules* **2011**, *44*, 2698−2706.
(35) Knaapila, M.; Evans, R. C.; Gutacker, A.; Garamus, V. M.; Székely, N. K.; Scherf, U.; Burrows, H. D. Conjugated Polyelectrolyte (CPE) Poly[3-[6-(N-methylimidazolium)hexyl]-2,5-thiophene] Complexed with Aqueous Sodium Dodecylsulfate Amphiphile: Synthesis, Solution Structure and "Surfactochromic" Properties. *Soft Matter* **2011**, *7*, 6863.
(36) Zhou, G.; Qian, G.; Ma, L.; Cheng, Y.; Xie, Z.; Wang, L.; Jing, X.; Wang, F. Polyfluorenes with Phosphonate Groups in the Side Chains as Chemosensors and Electroluminescent Materials. *Macromolecules* **2005**, *38*, 5416−5424.
(37) Li, X.; Chen, L.; Chen, Y.; Li, F.; Yao, K. Photocrosslinkable Liquid-crystalline Polythiophenes with Oriented Nanostructure and Stabilization for Photovoltaics. *Org. Electron.* **2012**, *13*, 104−113.
(38) Chen, M.; Wang, X.; Yu, Y. H.; Pei, Z. L.; Bai, X. D.; Sun, C.; Huang, R. F.; Wen, L. S. X-ray Photoelectron Spectroscopy and Auger Electron Spectroscopy Studies of Al-doped ZnO Films. *Appl. Surf. Sci.* **2000**, *158*, 134−140.
(39) Sun, Y.; Seo, J. H.; Takacs, C. J.; Seifter, J.; Heeger, A. J. Inverted Polymer Solar Cells Integrated with a Low-temperature-annealed Sol-gel-derived ZnO Film as an Electron Transport Layer. *Adv. Mater.* **2011**, *23*, 1679−1683.
(40) Shao, S.; Zheng, K.; Pullerits, T.; Zhang, F. Enhanced Performance of Inverted Polymer Solar Cells by Using Poly(ethylene oxide)-modified ZnO as an Electron Transport Layer. *ACS Appl. Mater. Interfaces* **2013**, *5*, 380−385.
(41) Braun, S.; Salaneck, W. R.; Fahlman, M. Energy-Level Alignment at Organic/Metal and Organic/Organic Interfaces. *Adv. Mater.* **2009**, *21*, 1450−1472.
(42) Woo, K.; Kim, Y.; Moon, J. A Non-toxic, Solution-processed, Earth Abundant Absorbing Layer for Thin-film Solar Cells. *Energy Environ. Sci.* **2012**, *5*, 5340−5345.
(43) Yasuda, H.; Sharma, A. K.; Yasuda, T. Effect of Orientation and Mobility of Polymer Molecules at Surfaces on Contact Angle and its Hysteresis. *J. Polym. Sci., Polym. Phys. Ed.* **1981**, *19*, 1285−1291.
(44) Ma, W.; Yang, C.; Gong, X.; Lee, K.; Heeger, A. J. Thermally Stable, Efficient Polymer Solar Cells with Nanoscale Control of the Interpenetrating Network Morphology. *Adv. Funct. Mater.* **2005**, *15*, 1617−1622.
(45) Xin, H.; Kim, F. S.; Jenekhe, S. A. Highly Efficient Solar Cells Based on Poly(3-butylthiophene) Nanowires. *J. Am. Chem. Soc.* **2008**, *130*, 5424−5425.
(46) Goh, C.; Kline, R. J.; McGehee, M. D.; Kadnikova, E. N.; Fréchet, J. M. J. Molecular-weight-dependent Mobilities in Regioregular Poly(3-hexyl-thiophene) Diodes. *Appl. Phys. Lett.* **2005**, *86*, 122110.
(47) Cheng, Y.-J.; Hsieh, C.-H.; Li, P.-J.; Hsu, C.-S. Morphological Stabilization by In Situ Polymerization of Fullerene Derivatives Leading to Efficient, Thermally Stable Organic Photovoltaics. *Adv. Funct. Mater.* **2011**, *21*, 1723−1732.
(48) Liu, Y.; Wan, X.; Wang, F.; Zhou, J.; Long, G.; Tian, J.; Chen, Y. High-performance Solar Cells Using a Solution-processed Small Molecule Containing Benzodithiophene Unit. *Adv. Mater.* **2011**, *23*, 5387−5391.
(49) Zhao, G.; He, Y.; Xu, Z.; Hou, J.; Zhang, M.; Min, J.; Chen, H.-Y.; Ye, M.; Hong, Z.; Yang, Y.; Li, Y. Effect of Carbon Chain Length in the Substituent of PCBM-like Molecules on Their Photovoltaic Properties. *Adv. Funct. Mater.* **2010**, *20*, 1480−1487.
(50) Liang, Z.; Zhang, Q.; Wiranwetchayan, O.; Xi, J.; Yang, Z.; Park, K.; Li, C.; Cao, G. Effects of the Morphology of a ZnO Buffer Layer on the Photovoltaic Performance of Inverted Polymer Solar Cells. *Adv. Funct. Mater.* **2012**, *22*, 2194−2201.
(51) Hayakawa, A.; Yoshikawa, O.; Fujieda, T.; Uehara, K.; Yoshikawa, S. High Performance Polythiophene/Fullerene Bulk-heterojunction Solar Cell with a TiOx Hole Blocking Layer. *Appl. Phys. Lett.* **2007**, *90*, 163517.
(52) Wei, Q.; Nishizawa, T.; Tajima, K.; Hashimoto, K. Self-organized Buffer Layers in Organic Solar Cells. *Adv. Mater.* **2008**, *20*, 2211−2216.

DOI: 10.1021/acsami.5b03340
ACS Appl. Mater. Interfaces 2015, 7, 19024−19033

(53) Gilot, J.; Wienk, M. M.; Janssen, R. A. J. Double and Triple Junction Polymer Solar Cells Processed from Solution. *Appl. Phys. Lett.* **2007**, *90*, 143512.
(54) Trost, S.; Zilberberg, K.; Behrendt, A.; Polywka, A.; Görrn, P.; Reckers, P.; Maibach, J.; Mayer, T.; Riedl, T. Overcoming the "Light-Soaking" Issue in Inverted Organic Solar Cells by the Use of Al:ZnO Electron Extraction Layers. *Adv. Energy Mater.* **2013**, *3*, 1437−1444.

DOI: 10.1021/acsami.5b03340
ACS Appl. Mater. Interfaces 2015, 7, 19024−19033